62. Belousov, V.I. et al., Intense microwave emission from periodic relativistic electron bunches, *Sov. Tech. Phys. Lett.*, 4, 584, 1978 (*Pis'ma Zh. Tekh. Fiz.*, 4, 1443, 1978).
63. Gunin, A.V. et al., Relativistic X-band BWO with 3-GW output power, *IEEE Trans. Plasma Sci.*, 26, 326, 1998.
64. Kitsanov, S.A. et al., Pulsed 5-GW resonance relativistic BWT for a decimeter wavelength range, *Tech. Phys. Lett.*, 29, 259, 2003 (*Pis'ma Zh. Tekh. Fiz.*, 29, 87, 2003).
65. Shiffler, D. et al., A high-power two stage traveling-wave tube amplifier, *J. Appl. Phys.*, 70, 106, 1991; Shiffler, D. et al., Sideband development in a high-power traveling-wave tube microwave amplifier, *Appl. Phys. Lett.*, 58, 899, 1991.
66. Kovalev, N.F. et al., Parasitic currents in magnetically insulated high-current diodes, *Sov. Tech. Phys. Lett.*, 3, 168, 1977 (*Pis'ma Zh. Tekh. Fiz.*, 3, 413, 1977).
67. Aleksandrov, A.F. et al., Broadening of a relativistic electron beam in Cerenkov-radiation source, *Sov. Tech. Phys. Lett.*, 14, 349, 1988 (*Pis'ma Zh. Tekh. Fiz.*, 14, 783, 1988).
68. Burtsev, V.A. et al., Generation of microsecond microwave pulses by relativistic electron beams, *Sov. Tech. Phys. Lett.*, 9, 617, 1983 (*Pis'ma Zh. Tekh. Fiz.*, 9, 1435, 1983).
69. Hahn, K., Fuks, M.I., and Schamiloglu, E., Initial studies of a long-pulse relativistic backward-wave oscillator using a disk cathode, *IEEE Trans. Plasma Sci.*, 30, 1112, 2002.
70. Korovin, S.D. et al., Pulsewidth limitation in the relativistic backward wave oscillator, *IEEE Trans. Plasma Sci.*, 28, 485, 2000.
71. Bugaev, S.P. et al., Collapse of a relativistic high-current electron beam during generation of high-power electromagnetic radiation pulses, *Radio Eng. Electron. Phys.*, 29, 132, 1984 (*Radiotekh. Elektron.*, 29, 557, 1984).
72. Korovin, S.D., Rostov, V.V., and Totmeninov, E.M., Studies of relativistic backward wave oscillator with low magnetic field, in *Proceedings of the 3rd IEEE International Vacuum Electronics Conference*, Monterey, CA, 2002, p. 53.
73. El'chaninov, A.S. et al., Highly efficient relativistic backward-wave tube, *Sov. Tech. Phys. Lett.*, 6, 191, 1980 (*Pis'ma Zh. Tekh. Fiz.*, 6, 443, 1980).
74. Tkach, Yu.V. et al., Microwave emission in the interaction of a high-current relativistic electron beam with a plasma-filled slow-wave structure, *Sov. J. Plasma Phys.*, 1, 43, 1975 (*Fiz. Plazmy*, 1, 81, 1975).
75. Carmel, Y. et al., Demonstration of efficiency enhancement in a high-power backward-wave oscillator by plasma injection, *Phys. Rev. Lett.*, 62, 2389, 1989.
76. Goebel, D.M., Schumacher, R.W., and Eisenhart, R.L., Performance and pulse shortening effects in a 200-kV PASOTRON HPM source, *IEEE Trans. Plasma Sci.*, 26, 354, 1998.

9

Klystrons and Reltrons

9.1 Introduction

The distinctive feature of *klystrons* and *reltrons* is that the microwave-generating interactions in these devices take place in resonant cavities at discrete locations along the beam. The drift tube connecting the cavities is designed so that electromagnetic wave propagation between the cavities is cut off; without electromagnetic coupling between cavities, they are coupled only by the bunched beam, which drifts from one cavity to the next. To guide the beam along the drift tube, an axial magnetic guide field is applied, so that klystrons and reltrons (in those instances where a magnetic field is applied) are O-type devices. By contrast, in other O-type devices, such as the Cerenkov sources, free-electron lasers, or gyro-devices, microwaves are generated by beam-wave resonances that transfer beam energy to a wave over an extended interaction space or in a series of electromagnetically coupled cavities. The attractions of klystrons are their high power and efficiency, potentially wide bandwidth, and phase and amplitude stability.

All of the truly high power klystrons are relativistic, with beam voltages of the order of 500 kV or higher. As we show in Figure 9.1, though, relativistic klystrons are clearly differentiated into two groups on the basis of the beam impedance and, as we shall see, the bunching mechanisms that accompany low- and high-impedance operation. *High-impedance klystrons*, with impedances of the order of 1 kΩ, operate much the same way as conventional klystrons, albeit at higher voltages. In most cases, high power klystrons in this class have been developed as drivers for the radio frequency linear accelerators (RF linacs) in high-energy electron-positron colliders. There are two subclasses of high-impedance klystrons: those that operate at mildly relativistic voltages near 500 kV and those that operate at fully relativistic voltages of 1 MV or more. *Low-impedance klystrons* with impedances of about 100 Ω or less, on the other hand, feature much higher space-charge forces, which provide for a uniquely powerful bunching mechanism.

The *reltron* is similar to klystrons in that microwave power is extracted from a bunched beam using a set of output cavities; however, it is unique

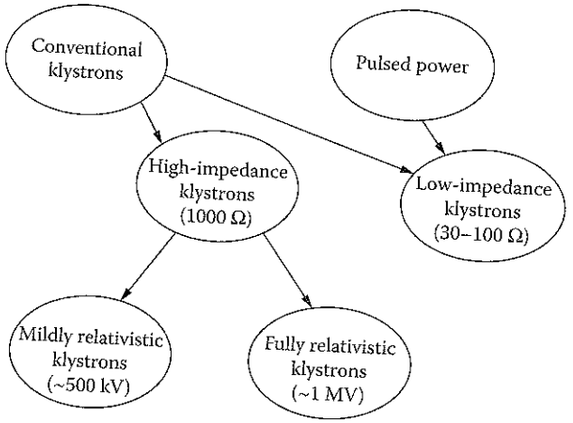

FIGURE 9.1
Classifying the different types of klystrons.

in two respects. First, the bunching mechanism differs from that in a klystron, and, second, the bunched beam is reaccelerated to higher energy to increase the energy withdrawn in the output cavities.

Representative performance parameters for the klystrons and the reltron are shown in Table 9.1. Note several features: (1) these devices are quite efficient by high power microwave (HPM) standards; (2) high power, high-impedance klystrons are optimized for very specialized application to RF linacs, where tunability is of limited interest; and (3) reltrons can be run without a magnetic field in some instances. High-impedance klystrons, particularly the mildly relativistic version, and the reltron are the most mature of the devices considered in this chapter. The klystron development efforts at the Stanford Linear Accelerator Center (SLAC) and at the High Energy Accelerator Research Organization (KEK) in Tsukuba, Japan, have created a line of highly optimized klystrons with power output of about 100 MW at frequencies from the S-band to the X-band. Similar technology might be scaled up to 1 GW if proposed multibeam versions were to be developed. Several versions of the reltron producing several hundred megawatts have been developed commercially for microwave effects testing at European laboratories, also over a wide range of frequencies that can be obtained through a mix of mechanical tuning and part change outs. Ultimately, the low-impedance klystron has generated the highest power, with proven performance of over 10 GW at 1.3 GHz. Using annular beams and a bunching mechanism that depends intrinsically on high beam currents, it offers the most potential for operation at gigawatt power levels.

TABLE 9.1

Representative Parameters for the Klystrons and Reltron

	Sources			
	High-Impedance Klystrons			
Source Parameters	**Mildly Relativistic Klystrons**	**Fully Relativistic Klystrons**	**Low-Impedance Klystrons**	**Reltrons**
Frequency range	2.856–11.4 GHz	11.4–14 GHz	1–3 GHz	0.7–12 GHz
Peak power	150 MW	100–300 MW	10–15 GW	600 MW
Electronic conversion efficiency	50–60%	35–50%	40%	40%
Pulse width	3 μsec	35 nsec	50–100 nsec	Up to 1 μsec
Tunable range	na	na	—	±15%
Repetition rate	60 Hz	na	na	10 Hz
Output mode	—	—	TM_{01}	TE_{10}
Bandwidth	Limited	Limited	—	0.1%
Voltage	~500 kV	~1 MV	~1 MV	~1–1.5 MV
Electrical impedance	~1 kΩ	200–400 Ω	30 Ω	~700 Ω
Magnetic field	0.2 T	0.5 T	1 T	—

9.2 History

Russell and Sigurd Varian invented the klystron in 1939, replacing the lumped-element L-C resonator of earlier devices with a resonant cavity in which fields interact directly with electron beams.[1] The Varian brothers derived the name *klystron* from the Greek verb *koyzo*, which describes the breaking of waves on a beach. The analogy is to the peaking of the electron density at the point of maximum bunching.

Through the 1940s, magnetrons were superior to klystrons in providing high power sources for radar. In the 1950s, though, klystron development was spurred by a growing understanding of the theory of space-charge waves and by the knowledge gained in the parallel development of traveling wave tubes. The basic configuration was scaled upward, and new design variants were introduced, most notably the *twystron* traveling wave hybrid amplifier and the *extended-interaction klystron*. Both use multiple cavities in the output section, which offers increased efficiency and bandwidth, as well as the added benefit of spreading the final interaction over a longer region to reduce the local fields and help prevent breakdown at high power.[2]

In the 1980s, the path to increased power split between high-impedance klystrons, either mildly or fully relativistic, and low-impedance klystrons. The high-energy physics community has been behind the development of high-impedance klystrons for their use as drivers in electron-positron colliders of increasingly higher energy. One branch of this effort is the so-called *SLAC klystron*, so named because the original S-band klystron of this type was developed at the Stanford Linear Accelerator Center, beginning in 1948, when a 30-MW, 1-μsec S-band klystron was developed for Stanford's Mark III linac.[3] In 1984, the Stanford accelerator was upgraded using 65-MW S-

band klystrons,[4] and the current version of this 2.856-GHz klystron produces 3.5-μsec pulses at 65 MW with a repetition rate of 180 Hz; at shorter pulse lengths, 100-MW output levels have been achieved.[5] In the mid-1990s, teams at SLAC and KEK produced a variety of klystrons that generated 150 MW in the S-band,[6] later improved in Germany to 200 MW,[7] and up to 100 MW in the X-band, at four times the original SLAC klystron frequency (11.424 GHz). The desire to reduce the overall electric power demand by a future 1-TeV accelerator that was referred to as the Next Linear Collider (NLC) led to one of the most notable technology advances for this tube, the development of a 75-MW tube with pulsed periodic magnet (PPM) focusing,[8] which eliminated the power demand by the electromagnet used in earlier versions. This line of klystron development stalled in August 2004, however, when the International Technology Recommendation Panel chose a competing technology from DESY (Deutsches Elektronen-Synchrotron) based on superconducting accelerating structures and lower-frequency, lower-power klystrons over the NLC concept for the future International Linear Collider, which has refocused klystron development in this direction.

Between the mid-1980s and mid-1990s, two groups focused on developing high-impedance klystrons operating at fully relativistic voltages. One group from the Lawrence Berkeley National Laboratory (LBNL) and the Lawrence Livermore National Laboratory (LLNL) explored an 11.424-GHz klystron as an alternative to the SLAC and KEK klystrons. Another group involving Russia's Joint Institute of Nuclear Research (JINR) in Dubna and the Budker Institute of Nuclear Physics (BINP) in Protvino investigated a 14-GHz driver for VLEPP, a Russian electron-positron collider concept.

The low-impedance relativistic klystron development traces to the high-current relativistic klystron amplifier (RKA) of Moshe Friedman, Victor Serlin, and coworkers at the Naval Research Laboratory (NRL) in the 1980s. Working at lower frequencies, in the L- and S-bands, they recorded power in excess of 10 GW in the mid-1990s. Motivated by a desire to push power levels still higher, they designed a triaxial version with an annular electron beam propagating within an annular drift space. The motivation was to increase the beam current while holding the current density relatively constant, and the triaxial configuration was intended to keep the cutoff frequency of the drift tube above the frequency of the microwaves generated. Workers at the Air Force Research Laboratory (AFRL) in Albuquerque and Los Alamos National Laboratory (LANL) took up triaxial RKA research in the late 1990s when the NRL effort halted.

The reltron grew out of early 1990s' investigations of the klystron-like *split-cavity oscillator* (SCO). Reltrons use the low-voltage bunching mechanism of the SCO, but then reaccelerate the bunched beam. This ordering, bunching at low voltage followed by further acceleration, somewhat reverses the order of acceleration and then bunching to take advantage of the greater ease of bunching at lower energies. Energy from the resulting high-energy bunched beam is extracted in klystron-like cavities. The reltron is used extensively for microwave effects studies in Germany, France, and Israel.

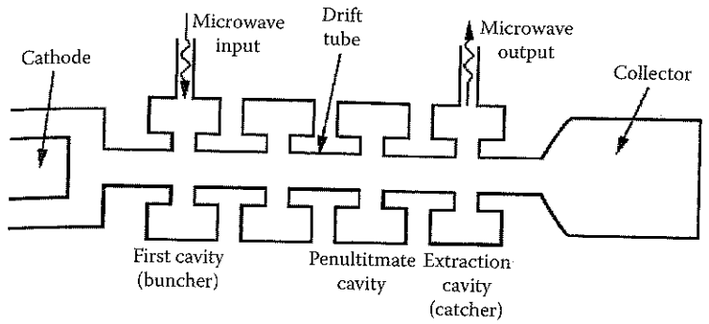

FIGURE 9.2
Basic configuration of a klystron.

9.3 Design Principles

Figure 9.2 shows a klystron in schematic form. The key elements are (1) the electron beam, (2) the axial magnetic field that guides the beam, (3) the interaction circuit, comprised of the cavities and the drift tube for the electron beam, (4) the input and output couplers for the microwaves, and (5) the beam collector. A microwave input signal excites a resonant electromagnetic mode of the first cavity. Each cavity has a gap that opens onto the drift tube, and electrons in the beam passing through the drift tube are accelerated or decelerated by the electric fields from the gap, depending on the phase of the fields as they pass by. Drifting between cavities, the faster electrons overtake the slower electrons, and charge bunches form on the beam. The drift tube separating the cavities is designed so that the electromagnetic fields do not propagate from one cavity to the next. Thus, communication between the cavities is via the bunched beam only. The fields excited in downstream cavities by the bunched beam enhance the bunching, so that the input signal is amplified in downstream cavities until the high power output signal is extracted from the final cavity.

As we shall show, there are some significant differences between the operating mechanisms of high-impedance klystrons, low-impedance klystrons, and reltrons. We therefore describe their operating and design principles in that order. First, though, we discuss the basic considerations in choosing the configuration of these devices.

9.3.1 Voltage, Current, and Magnetic Field

The electron beam is the energy source for the microwaves generated in a klystron. Let I_b be the beam current and V_0 the accelerating voltage for the

beam. In *high-impedance klystrons*, such as the SLAC klystron, pencil beams with circular cross sections are employed. The current is typically low enough that the energy of a beam electron, $\gamma_b mc^2$, can be approximated by the expression

$$\gamma_b \approx \gamma_0 \equiv 1 + \frac{eV_0}{mc^2} \tag{9.1}$$

Low-impedance klystrons, on the other hand, use thin, hollow beams with annular cross sections. Because they operate at higher currents, the beam space-charge creates a significant electric field between the beam and the wall. The potential energy in that electrostatic field reduces the beam kinetic energy, so that γ_b is lower than the value in Equation 9.1. In *low-impedance klystrons*, one finds γ_b by solving the equation[9]

$$\gamma_0 = \gamma_b + \frac{I_b}{I_s \beta_b} \equiv \gamma_b + \alpha \gamma_b^3 \tag{9.2}$$

where γ_0 is as defined in Equation 9.1 and $\beta_b = v_b / c = (1 - 1/\gamma_b^2)^{1/2}$. The factors I_s and α depend on the cross-sectional distribution of beam current; for a thin annular beam of mean radius r_b in a drift tube of radius r_0,

$$I_s = \frac{2\pi\varepsilon_0 mc^3}{e} \frac{1}{\ell n(r_0 / r_b)} = \frac{8.5}{\ell n(r_0 / r_b)} kA \tag{9.3a}$$

$$\alpha = \frac{I_b}{I_s \gamma_b^3 \beta_b} \tag{9.3b}$$

In solving Equation 9.2, one chooses the solution for γ_b that lies in the range $\gamma_0^{1/3} \le \gamma_b \le \gamma_0$. Note that as $r_b \to r_0$, $\alpha \to 0$ and $\gamma_b \to \gamma_0$; i.e., as the beam approaches the wall, the potential energy tied up in the electrostatic field in the space between the beam and the wall vanishes. This permits the high operating currents of the low-impedance klystrons, as well as high efficiencies, as long as the beam is kept near the wall (see Problems 1 to 6).

The magnetic field must be large enough to confine the beam within the drift tube and to keep the beam relatively stiff by preventing too much radial motion. For the pencil beams in high-impedance klystrons, the axial magnetic field required to confine the beam current is[10]

$$B_z(T) \overset{*}{=} \frac{0.34}{r_b(cm)} \left[\frac{I_b(kA)}{8.5 \beta_b \gamma_b} \right]^{1/2} \tag{9.4}$$

As noted in the reference, this is the field required to confine the beam to a radius r_b; however, one must also confine the RF current in the beam, which in a SLAC klystron can be about $4I_b$, so that, as a rule of thumb, the actual magnetic field should be about twice that in Equation 9.4 (see Problem 7).

9.3.2 Drift Tube Radius

The radius of the drift tube is limited by the requirement that the drift tube be cut off to the propagation of electromagnetic modes between cavities. As we showed in Chapter 4, the mode with the lowest cutoff frequency in a cylindrical waveguide of radius r_0 is the TE_{11} mode, for which the cutoff frequency is

$$f_{co}(TE_{11}) = \frac{\omega_{co}}{2\pi} = \frac{1}{2\pi}\left(\frac{1.84c}{r_0}\right) = \frac{8.79}{r_0(cm)} \ GHz \tag{9.5}$$

with c the speed of light. Since the operating frequency of the klystron must lie below this value, i.e., $f < f_{11}$, the radius of the drift tube is limited by the relation

$$r_0(cm) < \frac{8.79}{f(GHz)} \tag{9.6}$$

Thus, the maximum drift tube radius must decrease as the frequency increases. As an example, at 1 GHz, the upper limit on the drift tube diameter is about 17.6 cm, while at 10 GHz, the limit is 1.76 cm (see Problems 8, 9, and 10).

9.3.3 Klystron Cavities

Figure 9.3 shows examples of cavities used in high power klystrons; the cavity in Figure 9.3a is commonly used in SLAC klystrons, while that in Figure 9.3b is used in the low-impedance klystrons. Klystron cavities operate much like a lumped-element LC oscillator, as indicated by the model in Figure 9.4. Imagine that a pair of highly transmitting meshes with spacing d are placed across the beam tube at the gap and that a time-varying electric field $Ee^{-i\omega t}$ is imposed across the gap. The field induces a time-varying charge on each mesh with amplitude q = CV = C(Ed), where C is the capacitance of the gap between the meshes and V is the voltage, with E assumed constant across the gap. As the charge flows between meshes, a current I flows though the wall of the cavity as shown, creating a magnetic field B. Thus, the gap acts like a capacitance, while the current-carrying walls of the cavity act like an inductor of inductance L, and the series combination of the two, driven by the electron beam, is an LC oscillator.

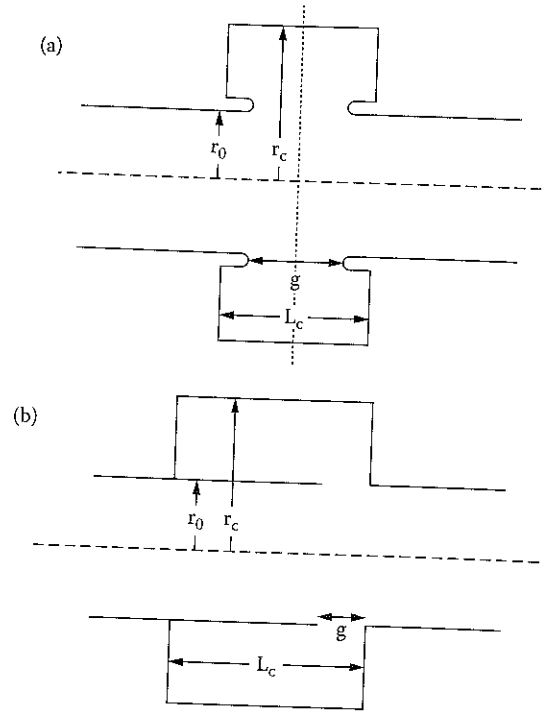

FIGURE 9.3
Cavities commonly used in high power klystrons: (a) a cavity used in a SLAC klystron; (b) a cavity commonly seen in low-impedance klystrons.

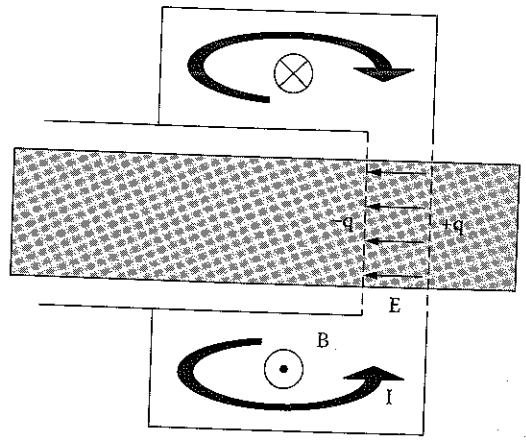

FIGURE 9.4
Model for visualizing a klystron cavity as an LC oscillator.

In terms of the length of a cavity, using the notation of Figure 9.3b, the two extremes are a *pillbox cavity*, with $L_c < (r_c - r_0)$, and a *coaxial cavity*, with $L_c > (r_c - r_0)$. In the latter case, for relatively long cavities with $L_c >> (r_c - r_0)$, they can be modeled as a transmission line of characteristic impedance $Z_0 = 60 \ln(r_c/r_0)\ \Omega$, terminated on one end by a short circuit, representing the closed end of the cavity, and at the other end by a capacitance C, representing the cavity gap capacitance. One can show[11] that for a small gap capacitance, with $Z_0\omega C << 1$, the cavity length is approximately given by

$$L_c\,(cm) \approx (2n+1)\frac{\lambda}{4} = (2n+1)\frac{7.5}{f\,(GHz)}\ ,\ n = 0, 1, 2, \ldots \qquad (9.7)$$

Here, $\lambda = c/f$, and the lowest-order axial mode has $n = 0$ (see Problem 11).

In designing a cavity, one chooses the dimensions and wall materials in order to meet a number of different, and sometimes competing, design criteria. The cavity must be resonant at the operating frequency of choice. Its quality factor, Q, must be low enough that the cavity has the desired bandwidth (since $Q \approx f/\Delta f$, with Δf the bandwidth) and that oscillations can build up on a timescale less than the duration of the electron beam (because, alternatively, one can write $Q \approx \omega E_s/\Delta P$, where E_s is the energy stored in the cavity and ΔP is either the power lost per cycle, which depends on both losses to the wall and the effective loss associated with the buildup of the gap field, or the energy input per cycle required to build up the energy E_s, in which case $Q \approx \omega\tau_B$, with τ_B the time for the buildup of oscillations), but high enough in the case of the input cavity that the input power required to modulate the beam be practical. In addition to Q, one designs the cavity to manage the field magnitudes at the wall and in the gap in order to prevent breakdown.

We compute the desired cavity parameters by solving the electromagnetic field equations. This can be done analytically using some approximations; for example, the fields for the cavity of Figure 9.3a, both inside the cavity and in the drift tube outside, were solved under the approximation that the electric field across the gap be a constant, equal to V_g/g, with V_g the gap voltage.[12] Historically, the characteristics of klystron cavities of the type shown in Figure 9.3b were computed and presented in graphs as functions of the ratios L_c/r_0, g/r_0, and r_c/r_0, with frequencies normalized to c/r_0.[13] Today, however, cavities are typically designed — or cavity designs are refined — using numerical tools such as the code SUPERFISH.[14]

In a multicavity klystron, individual cavities can be separately tuned to maximize gain, efficiency, or bandwith.[15] To maximize gain, each of the cavities is synchronously tuned with the desired signal frequency. To maximize efficiency, bunching is initiated with a set of synchronously tuned cavities, following which one or more of the cavities preceding the final cavity, most notably the penultimate cavity, is tuned upward in frequency so that at the signal frequency ω it appears to be inductive. Consequently,

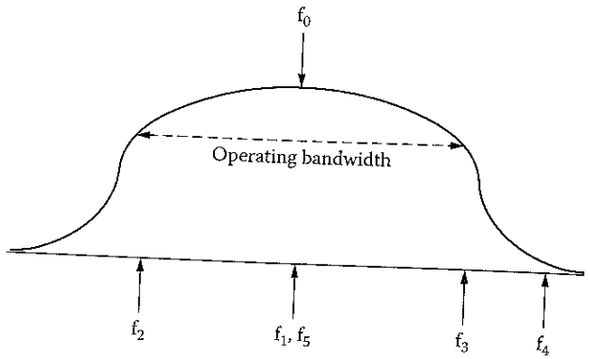

FIGURE 9.5
Qualitative relationship between tuning frequencies for a broadband five-cavity klystron amplifier. Frequencies f_1 and f_5 are for the input and output cavities, respectively, while f_4 is for the penultimate cavity.

the relative phasing of voltage and current is such that electrons in front of a bunch are decelerated, pushing them into the bunch, while electrons trailing a bunch are accelerated, again enhancing the bunching. Thus, the signal in the output cavity is increased in magnitude. Finally, to maximize bandwidth, the intermediate cavities are *stagger tuned* about the central frequency, while the penultimate cavity is tuned upward to enhance bunching, and the output cavity is designed to have wide bandwidth. This tuning scheme is illustrated in Figure 9.5.

In high power klystrons, the electric fields in the output cavity can be many times greater than the breakdown strength, so that the challenge for the designer is to increase the breakdown strength of the output cavity. One design technique that reduces the electric fields in the output section is the use of *extended-interaction* or *traveling wave* output sections, as shown in Figure 9.6. In the former, a small number of cavities with larger gaps are used in place of the single cavities of a conventional klystron. In the latter, the usual bunching cavities are used to generate the signal current on the beam, from which microwave energy is coupled out over a much longer traveling wave section, which is composed of coupled cavities in the figure. Note the dummy load on one end of the traveling wave section to prevent reflections and the buildup of oscillations, while the signal is coupled out on the other end.

9.3.4 Electron Velocity Modulation, Beam Bunching, and Cavity Spacing

The modulation of electron velocities by the electric field from the cavity gaps initiates the process that creates charge bunches on the beam downstream of the cavity. Interestingly, until the gap voltage becomes quite large and the bunching process becomes nonlinear, the evolution of the bunches

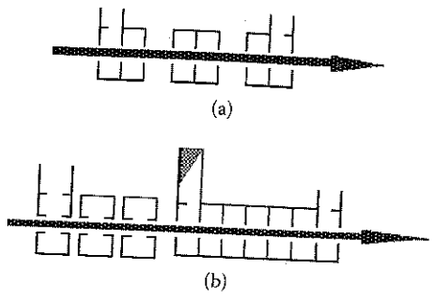

FIGURE 9.6
(a) Extended-interaction and (b) traveling wave structures for klystrons.

is governed by the intrinsic properties of the beam — specifically the electron energy and velocity, and the current density and beam distribution — while the magnitude of the bunching is determined by the intensity of the modulation, which of course is determined by the gap voltage. In this section, we will consider velocity modulation and the bunching process for a simple model relevant to classical, high-impedance klystrons.

To understand electron velocity modulation by the time-varying electric field in the gap of classical klystrons, return to our simplified one-dimensional model of Figure 9.4, ignoring the transverse dimensions and fields in the gap and, to lowest order, the electric field resulting from the beam's space-charge. An electron of charge –e and mass m entering the gap of width g at $t = t_1$ with velocity v_b leaves the gap with velocity $v_b + v_1$, where

$$v_1 = -\frac{eEg}{m\gamma_b^3 v_b} M e^{-i\omega(t_1+\Delta t/2)} \tag{9.8}$$

Here, $\gamma_b = [1 - (v_b/c)^2]^{-1/2}$, $\Delta t = g/v_b$ is the travel time across the gap, and

$$M \equiv \frac{\sin\left(\frac{\omega\Delta t}{2}\right)}{\left(\frac{\omega\Delta t}{2}\right)} \tag{9.9}$$

is the *modulation factor* for a uniform electric field, which is the same for every electron (see Problems 12 and 13). M takes account of the phase average of the time-varying force on an electron as it transits the planar gap, and the form in Equation 9.9 is specific to our assumption that E is constant across the gap. Three points are significant here. First, the magnitude of the modulation is proportional to the gap voltage $V_g = Eg$. Second, the factor γ_b^3 in the denominator of Equation 9.8 rapidly increases the difficulty of perturbing

the beam velocity as the beam energy increases. Third, the combination $(g/v_b)M$ is purely sinusoidal in the gap travel time, Δt, with zeroes at $\omega\Delta t = 2n\pi$ $(n \geq 1)$, implying that the velocity of an electron is unchanged as it exits the gap if its travel time is one period of the oscillating field (see Problem 14 to consider alternatives to this modulation factor).

The formation of charge bunches on a velocity-modulated beam is a periodic process. Leaving the gap, the faster electrons overtake the slower electrons and bunches begin to form. Bunch formation is countered by the buildup of space-charge forces as the charge density in a bunch increases, however, and space-charge repulsion eventually causes debunching. The process is like that of compressing and later releasing a spring. The time and distance scale for bunch formation is determined by the interaction of the fast and slow space-charge waves on the beam, which in our simple one-dimensional model have the dispersion relation

$$\omega = k_z v_b \pm \frac{\omega_b}{\gamma_b} \tag{9.10}$$

where the + sign goes with the fast space-charge wave and the – sign with the slow. In this expression, $\omega_b = (\rho_b e/\varepsilon_0 m\gamma_b)^{1/2}$ is the relativistic beam plasma frequency (with ε_0 the permittivity of free space and ρ_b the magnitude of the charge density on the beam), which depends, as we mentioned earlier, only on the properties of the beam, and not on the strength of the modulation. In the small-signal, linear regime of operation, the interaction of these two waves sets the distance from the cavity at which bunching reaches a maximum:

$$z_b = \frac{\pi\gamma_b v_b}{2\omega_b} \equiv \frac{\lambda_b\gamma_b}{4} \propto \frac{\gamma_b^{3/2} v_b^{3/2}}{J_b^{1/2}} \tag{9.11}$$

where $\lambda_b = 2\pi v_b/\omega_b$ and J_b is the beam current density (see Problems 15 and 16). Beyond z_b, the beam debunches, and at $z = 2z_b$, the bunch disappears. The *Applegate diagram* of Figure 9.7, which takes account of space-charge repulsion,[16] shows the trajectories of individual electrons to illustrate this phenomenon. Equation 9.11 shows us that there is a strong increase in bunching distance with the beam energy, as well as a decrease as the beam current density increases. When the beam is generated in a Child–Langmuir diode at voltage V_0 (see Section 4.6.1), we can simplify the scaling still further in the nonrelativistic limit, where $\gamma_b \sim 1$, $v_b \propto V_0^{1/2}$, and $J_b \propto V_0^{3/2}$, to see that z_b is approximately independent of V_0 at low voltage; in the ultrarelativistic limit, however, $\gamma_b \propto V_0$, $v_b \sim c$ and $J \propto V_0$, so that $z_b \propto V_0$.

The key, of course, is to locate each successive cavity near a maximum for bunching from the previous cavity. Because of the importance of this fact, consider several real-world modifications of our simple explanation of modulation and bunching in classical, high-impedance klystrons (in the next section, we will consider the unique features of low-impedance, relativistic klystrons). For example, real klystron accelerating gaps are not bounded by grids, and real electron beams have finite radial extent. Thus, the effective axial length of the gap is lengthened a bit because the gap equipotential lines bulge near the axis of the drift tube. Without the grids, which short out radial electric fields, and considering the finite radial extent of the beam, the modulation factor of Equation 9.9 must be replaced by the product of axial and radial modulation factors: $M \rightarrow M_a M_r$. The exact form of M_a and M_r depends on the configuration details.[17] In the particular case of a hollow electron beam of radius r_b, for an accelerating cavity like that shown in Figure 9.3a,

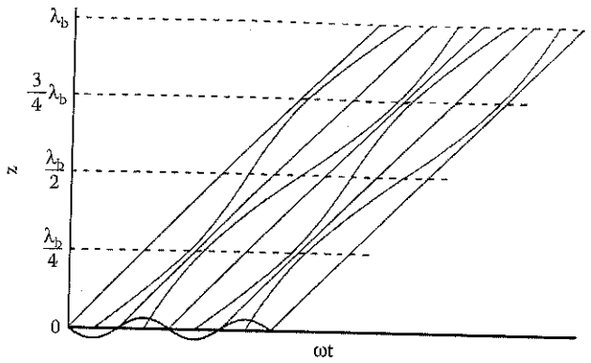

FIGURE 9.7
Applegate diagram taking account of space-charge repulsion within the bunches. The plot is for a nonrelativistic system with λ_b set to unity. (From Gilmour, A.S., Jr., *Microwave Tubes*, Artech House, Dedham, MA, 1986, p. 229. With permission.)

$$M_r = J_0(k_0 r_0)\frac{I_0(\theta_b)}{I_0(\theta_0)} \tag{9.12}$$

with $k_0 = 2\pi f/c$, $\theta_b = k_0 r_b/(\gamma_b\beta_b)$, and $\theta_0 = k_0 r_0/(\gamma_b\beta_b)$.[12]

In considering space-charge effects, we note that image charges on the walls of the drift tube reduce the effective value of the beam plasma frequency to a value $\omega_q < \omega_b$. A number of publications present computed values for the reduced plasma frequency.[18,19] The effect of the reduced plasma frequency is to increase z_b in Equation 9.11, and thus the spacing between klystron cavities.

Countering the tendency of the reduced plasma frequency to extend the distance over which bunching peaks, nonlinear effects tend to decrease that distance, as indicated in Figure 9.8. There we can see that the signal current induced on the beam by a first cavity at $z = 0$ peaks at a distance given by Equation 9.11, modified by replacing ω_b with ω_q. Placing a second cavity at z_b creates a stronger modulation that causes the signal current to peak over

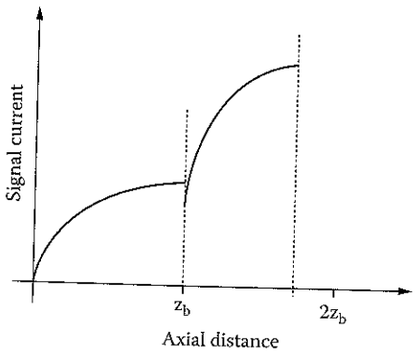

FIGURE 9.8
Nonlinear bunching effects downstream of a second cavity, with the first and second cavities located at $z = 0$ and z_b.

a shorter distance. The reason is that nonlinearities in the modulation process at higher gap voltages create high-energy electrons that overcome the space-charge repulsion force to maximize the signal current component over a shorter distance than the small-signal theory would indicate.[20]

We have also ignored radial motions of the beam to this point, which amounts to an assumption of a strong guiding magnetic field in the axial direction. As the magnetic field is reduced toward the *Brillouin limit*, where the magnetic field is just large enough to counter the space-charge expansion forces, space-charge bunching manifests itself as a modulation in the diameter of the beam also, which tends to reduce the effective beam plasma frequency still further and increase the distance between cavities.[21]

9.3.5 Beam Bunching in Low-Impedance Relativistic Klystrons

The bunching mechanisms in low-impedance relativistic klystrons are particularly intense, so that such devices typically consist of only two bunching cavities plus an extraction cavity. In fact, as we shall see shortly, the bunching mechanisms in the two cavities differ from one another in very significant ways.

The bunching mechanism in the first cavity is similar to that of classical klystrons: velocity modulation in the gap triggers the interaction of the space-charge waves on the beam, which determines the distance over which bunching takes place. A key difference, however, is that the frequencies of the fast and slow space-charge waves on an intense relativistic electron beam in a waveguide are not shifted symmetrically above and below the beam line, $\omega = k_z v_b$, as indicated by the one-dimensional result in Equation 9.10. Rather, as Briggs showed for long wavelengths (i.e., small k_z),[22] the space-charge waves propagating below the cutoff frequency of a waveguide have a dispersion relation given by

$$\omega = k_z v_b \left(\frac{1 \pm \alpha\mu}{1 + \alpha} \right) \tag{9.13}$$

where α is given in Equation 9.3b for a thin hollow beam and

$$\alpha\mu = \frac{1}{\beta_b} \left(\alpha^2 + \frac{\alpha}{\gamma_b^2} \right)^{1/2} \tag{9.14}$$

In solving Equation 9.13, remember that one must also solve Equation 9.2 at the same time to find γ_b and β_b if the known quantities for a given system are the beam current I_b and the anode–cathode voltage in the diode V_0. Using these relations, the bunching maximum downstream of the first cavity is found to be[23]

$$z_b = \frac{\beta_b^2 - \alpha}{4\left(\alpha^2 + \alpha / \gamma_b^2\right)^{1/2}} \left(\frac{c}{f} \right) \tag{9.15}$$

The scaling here obviously differs from that in Equation 9.11, derived in one dimension for a solid beam in a classical high-impedance klystron, in that the bunching length depends on the frequency f (see Problem 17). Other, more subtle differences in scaling exist as well, but the most unique feature of the bunching in low-impedance relativistic klystrons is that, as shown in the reference, because of the asymmetric frequency shift of the two space-charge waves, the alternating current (AC) components of the beam current and voltage are partially in phase, whereas in the case considered in the last section, they are out of phase by 90°. As a result, in the case at hand, a portion of the direct current (DC) energy of the beam is converted to AC kinetic energy, which is in turn converted to electromagnetic energy of the microwaves, a direct DC-to-microwave process that does not occur in traditional high-impedance, low-current, and low-voltage klystrons.

The bunching process in the second cavity is more unique yet. The strength of the fields excited by the bunched beam arriving from the first cavity significantly alters the beam dynamics, creating a gating effect that basically adds an additional bunching effect that occurs right in the cavity. To understand this process, we rewrite Equation 9.2 with an additional term on the right to take account of the modification of the electrons' energies by the AC gap voltage V_1:

$$\gamma_0 = \gamma_b + \frac{I_b}{I_s \beta_b} + \frac{|e| V_1}{mc^2} \sin(\omega t) \tag{9.16}$$

One can show that when V_1 exceeds a threshold value,

$$V_1 \sin(\omega t) > V_{th} \tag{9.17}$$

with

$$V_{th} = \frac{mc^2}{|e|}\left\{\gamma_0 - \left[1 + \left(\frac{I_b}{I_{SCL}}\right)^{2/3}\left(\gamma_0^{2/3} - 1\right)\right]^{3/2}\right\} \tag{9.18}$$

the solution for γ_b and β_b in Equation 9.16 breaks down (see Problem 18). In this equation, I_{SCL} is the space-charge-limiting current discussed in Section 4.6.3, the maximum beam current that can propagate through a drift tube of radius r_0; for a thin annular beam of radius r_b (see Problems 22 and 23),

$$I_{SCL} = \frac{8.5}{\ell n(r_0 / r_b)}\left(\gamma_0^{2/3} - 1\right)^{3/2}$$

When the inequality in Equation 9.17 holds, additional current bunching arises at the output of the gap.[24] This additional AC component at the exit of the second gap is estimated to be $I_{1,exit} = I_b(2/\pi)(1 - V_{th}^2 / V_1^2)^{1/2}$, which is plotted in Figure 9.9. The contribution to the AC current from the second gap rises rapidly as V_1 exceeds V_{th}, asymptotically approaching a maximum of about 0.64. Additional velocity modulation in the gap further bunches the beam downstream.

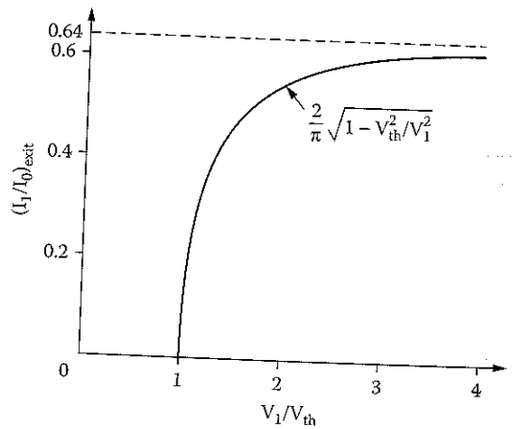

FIGURE 9.9
Current modulation at the exit of the second gap of a low-impedance klystron as a function of the gap voltage. The notation I_0 in the figure, from the reference, corresponds to the notation I_b used in the text. (From Lau, Y.Y. et al., *IEEE Trans. Plasma Sci.*, 18, 553, 1990. With permission.)

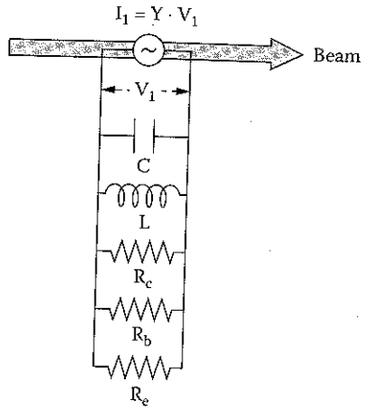

FIGURE 9.10
Lumped-element model of a klystron cavity and its coupling to the beam.

9.3.6 Circuit Modeling of Klystrons

While the detailed design of klystron cavities and beam tubes involves the use of computer codes that accurately model the electron beam dynamics, many times the properties of the cavities are described in terms of — and the parametric modeling of multicavity klystrons makes use of — lumped-element circuit models. The model for an individual cavity is as shown in Figure 9.10. The inductance and capacitance are arranged in parallel with three resistances: a beam resistance R_b, a cavity resistance R_c, and an external resistance R_e. These resistances represent, respectively, coupling to the beam, to the resistive cavity walls, and out of the cavity through openings or to external absorbers. The AC component of the gap voltage V_1 is related to the AC component of the beam current I_1 by Ohm's law:

$$I_1 = YV_1 = \frac{1}{Z}V_1 \tag{9.19}$$

where the cavity impedance Z (or admittance Y) is the parallel combination of the shunt impedances in the cavity:

$$Z = \frac{R}{1 + iQ\dfrac{\omega^2 - \omega_0^2}{\omega\omega_0}} = \frac{R}{Q}\frac{1}{\left(\dfrac{1}{Q} + i\dfrac{\omega^2 - \omega_0^2}{\omega\omega_0}\right)} \tag{9.20}$$

with R the parallel combination of R_b, R_c, and R_e. In Equation 9.20, the cavity inductance and capacitance have been replaced by the resonant frequency ω_0 and the cavity quality factor, Q:

$$\omega_0 = (LC)^{-1/2} \tag{9.21}$$

$$Q \equiv \omega_0 \tau_{RC} = \omega_0 RC \tag{9.22}$$

(see Problems 19 and 20). On the right side of Equation 9.20, we have pulled out the characteristic impedance,

$$Z_c \equiv \frac{R}{Q} \approx \frac{1}{\omega C} \tag{9.23}$$

which is a constant factor for a given cavity geometry in the absence of the beam.[25] The cavity impedance in Equation 9.20 peaks at R when the cavity is resonant, with $\omega = \omega_0$, and drops off away from this frequency with a sharpness dictated by the size of the quality factor, Q.

To sketch out the overall behavior of a multicavity klystron, we generalize the model of Figure 9.10 and model each cavity as shown in Figure 9.11, with an inductance and capacitance, denoted for the mth cavity, L_m and C_m,

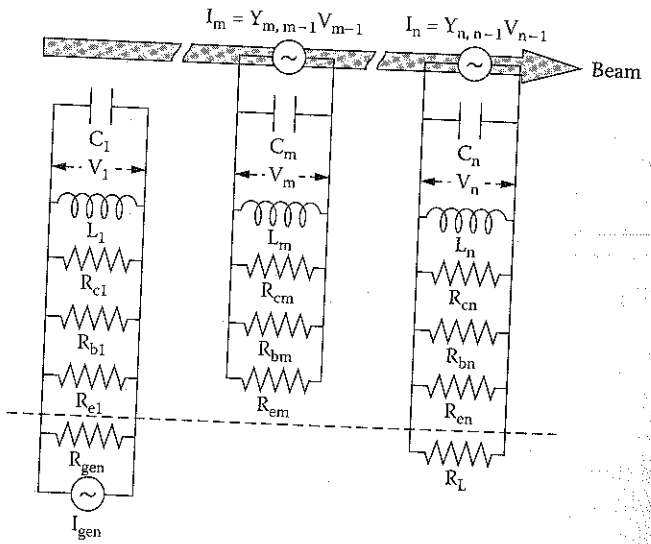

FIGURE 9.11
Lumped-element model for a multicavity klystron, with cavity 1 the input cavity, cavity m representative of an intermediate cavity, and cavity n the output cavity.

plus three parallel resistances, a beam resistance R_{bm}, a cavity resistance R_{cm}, and an external resistance R_{em}. The current source I_{gen} with shunt resistance R_{gen} represents the driving signal source for the klystron. It excites a gap voltage V_1 from the current flow through the cavity impedance. If the cavity is impedance matched to the generator, then $R_{gen} = Z_1$ and

$$V_1 = \frac{1}{2} I_{gen} Z_1$$

and the input power to the first cavity is

$$P_{in,\max} = \frac{1}{2}\left|\frac{I_{gen}}{2}\right|^2 R_{gen} = \frac{1}{2}\left|\frac{V_1}{Z_1}\right|^2 R_{gen} \tag{9.24}$$

This voltage, in combination with time-of-flight effects for the velocity-modulated beam as it travels to the second cavity, creates a signal current in the second cavity,

$$I_2 = Y_{21} V_1 \tag{9.25}$$

where, in the linear approximation for high-impedance klystrons, the transadmittance from cavity 1 to cavity 2, Y_{21}, is given by[26]

$$Y_{21} = i\frac{4\pi}{Z_0}\left[\frac{I_0(kA)}{17}\frac{1}{(1+s)\beta_b\gamma_b}\right]^{1/2} \sin(k_b d)\, e^{i\omega d/v_b} \tag{9.26}$$

with $Z_0 = 377\ \Omega$ the impedance of free space, $s = 2\ell n(r_0 / r_b)$, and

$$k_b = \frac{2\omega}{3c}\left[(1+s)^{1/2} - s^{1/2}\right]\left[\frac{17}{I_b(kA)}(\beta_b\gamma_b)^5\right]^{1/2} \tag{9.27}$$

Now I_2 excites a voltage V_2 in the second cavity via a relation like that in Equation 9.19. One thus proceeds iteratively using Ohm's law in each cavity to get the voltage and Equation 9.26 to get the current in the next cavity until one reaches the last cavity. At that point, one can collect all of the calculations performed previously to express the current in the last, or nth, cavity in terms of the voltage on the first,

$$I_n = Y_{n1} V_1 \tag{9.28}$$

Assuming that the load resistance R_L is matched to the final cavity, so that $R_L = Z_n$, the output power into R_L can be written

$$P_{out} = \frac{1}{2}\left|\frac{I_n}{2}\right|^2 R_L = \frac{1}{2}\left|\frac{Y_{n1}V_1}{2}\right|^2 R_L \tag{9.29}$$

Combining Equations 9.24 and 9.29, we thus find the gain G for the klystron in the linear regime of operation to be

$$G = \frac{P_{out}}{P_{in,\max}} = \frac{|Y_{n1}|^2 |Z_1|^2 R_L}{4R_{gen}} \tag{9.30}$$

9.3.7 Reltron Design Features

The reltron concept is as follows:[27] create a bunched beam at low voltage and then accelerate the electron bunches to relativistic velocities. As we see in Equations 9.11 and 9.15, this order of events makes the bunching easier. Further, the postaccelerated electrons will all be traveling at the same velocity, approximately the speed of light, so that velocity differences within the bunch become insignificant; the bunching created at low voltage in the first cavity is thus "frozen in." Because of the stiffness of the relativistic beam to deceleration, energy can be extracted over several cavities, which reduces the gap voltage per cavity and the chances of breakdown.

In addition to the postacceleration of the bunched beam, the reltron is also distinguished by a special bunching mechanism that, like the low-impedance klystron and the split-cavity oscillator (SCO),[28] is enabled by the use of intense electron beams at currents that lie close to the space-charge-limiting current. The reltron schematic is shown in Figure 9.12, and the bunching

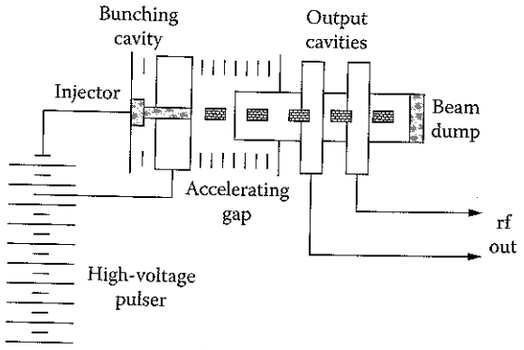

FIGURE 9.12
Schematic of the reltron. (From Miller, R.B. et al., *IEEE Trans. Plasma Sci.*, 20, 332, 1992. With permission.)

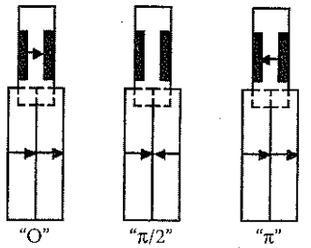

FIGURE 9.13
Lowest-order operating modes of the reltron bunching cavity. (From Miller, R.B. et al., *IEEE Trans. Plasma Sci.*, 20, 332, 1992. With permission.)

cavity and its three normal modes — 0, π/2, and π — are shown in Figure 9.13. The bunching cavity consists of two pillbox cavities coupled through magnetic slots to a third, side-mounted cavity. The electron beam passes only through the two pillbox cavities. The π/2-mode is unstable, so when the electron beam is injected, the electromagnetic fields in the cavities grow at the expense of the beam energy. When the beam current is an appreciable fraction of the space-charge-limiting current, a phenomenon formally similar to that in low-impedance klystrons comes into play, with the electrons essentially gated by the gap potential.

9.4 Operational Features

In the previous section, we discussed the design principles for high power klystrons and reltrons from a theoretical standpoint. In this section, we consider the operational features of actual devices that have been built and operated. We choose examples drawn from the three different types of devices: high-impedance klystrons employing pencil beams and operating at both near-relativistic and relativistic voltages to produce peak powers of roughly 100 MW; low-impedance klystrons employing intense annular beams to produce peak powers in excess of 1 GW; and reltrons that have produced hundreds of megawatts of power in pulses approaching 1 μsec.

9.4.1 High-Impedance, Near-Relativistic Klystrons

The development of this class of klystrons at SLAC and KEK in support of the NLC concept[29] placed a premium on phase stability, reliability, and cost, including both the capital cost of building the klystrons and the operating cost of the electricity, which in turn is affected by the klystron efficiency and magnet power demand. Although the NLC concept lost out in the competition for the International Linear Collider, the SLAC and KEK klystrons

TABLE 9.2

Key Parameters for the First of Two 150-MW S-band Klystrons Delivered by SLAC to DESY

Beam voltage	535 kV
Beam current	700 A
Beam microperveance	1.78×10^{-6} A/V$^{3/2}$
RF pulse width at rep rate	3 μsec at 60 Hz
Cathode current density	6 A/cm^2 (max)
Cathode convergence	40:1 (13.3-cm drift-tube diameter)
RF output power	150 MW
Cavity gradients	<360 kV/cm
Saturated gain	~55 dB
Efficiency	40%
Operating frequency	2.998 GHz
Solenoidal magnetic focusing field	0.21 T

remain the highest-power pulsed tubes based on conventional microwave tube technology. To illustrate the features of the devices, we concentrate here on two particular device types: (1) the 150-MW S-band klystrons built by SLAC for DESY, the highest-operating-power klystrons from SLAC, and (2) the 11.424-GHz klystrons developed at SLAC using periodic permanent magnet (PPM) focusing of the electron beam to save on power otherwise expended on an electromagnet.

To give a sense of scale, the 150-MW tubes were about 2.6 m long, with a mass of about 300 kg.[7] Key parameters for the first of the tubes delivered to DESY are shown in Table 9.2.[30] Note first that the voltage is rather high for such a tube, exceeding 500 kV. Second, the cathode current density available from the M-type dispenser cathode originally used for this tube, 6 A/cm^2 or less, forced the designers to compress the solid-beam radius by a 40:1 ratio to reduce it to fit the 13.3-cm diameter drift tube. Lifetime issues later dictated a switch to a scandate cathode. Third, the saturated gain is quite high, about 55 dB. Designers conducted numerical simulations using a 2-dimensional particle-in-cell (PIC) code to fine-tune the cavity placements and frequencies, in the latter instance allowing designers to stagger the first six nonfundamental modes of the cavities to reduce the chances of self-oscillation. Nevertheless, additional work was required to deal with parasitic oscillations in the tube, including the later replacement of a section of the copper drift tube with a threaded and sandblasted stainless steel drift tube to increase signal losses between cavities. Fourth, in order to improve upon the greater than 40% efficiency in this first tube, the second tube featured a two-cell output cavity (an extended-interaction configuration) and an efficiency of about 50%. Finally, the magnetic field of 0.21 T produced by the 15-kW solenoidal field coil surrounding the klystron is about three times the minimum Brillouin field needed to confine and guide the electron beam through the tube.

In later experiments at DESY, the second tube was operated at over 200 MW of peak power in a 1-μsec pulse.[7] This higher power was achieved by

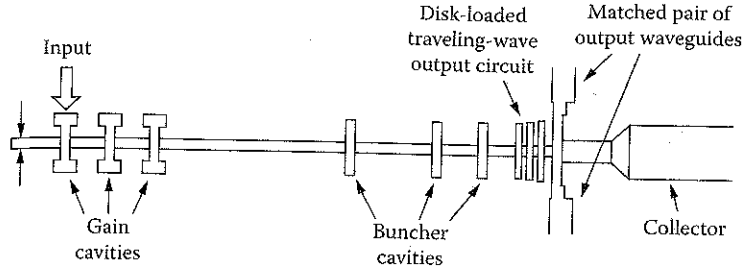

FIGURE 9.14
Configuration for the SLAC 75-MW klystron using a solenoidal magnetic field coil.

raising the operating voltage and current to 610 kV and 780 A, which necessitated an increase in the guiding magnetic field by about 6%.

Concern for the power consumption of solenoidal field magnets in a projected NLC demanding thousands of klystrons first drove SLAC designers, and later designers at KEK, to develop an 11.424-GHz klystron with a PPM magnetic focusing system for the beam. The permanent magnets, which alternate in polarity to reduce their required size and weight,[31] produce a periodically varying magnetic field on axis for which the period must be small compared to the plasma wavelength on the beam for proper focusing (see the discussion surrounding Equation 9.11 and later discussion of the modification of the idealized one-dimensional value by two-dimensional effects in a drift tube). The disadvantage of the magnets is the lack of flexibility that goes with being unable to change the currents in coils to adjust field profiles and strengths without disassembling the tube.

Versions of PPM klystrons rated at 50 and 75 MW have been designed and built. Their configuration is essentially the same as that shown in Figure 9.14, which is that for a 75-MW klystron using a solenoidal field coil.[32] From the left in the figure, the first three cavities are reentrant to enhance the characteristic impedance, R/Q, and are stagger tuned to increase the klystron bandwidth. The next three to the right are pillbox cavities tuned well above the operating frequency to enhance bunching and final output power, as discussed in the previous section. The final cavity is a disk-loaded traveling wave section: four cells for the klystron with the solenoidal coil and five for the PPM klystron. These traveling wave sections spread the power across several cells, reducing the electric fields and preventing breakdown. The added cell in the case of the PPM klystron is a result of the lower perveance of that tube, which reduces the coupling to the cavity. The SLAC PPM klystron itself is shown in Figure 9.15.[33]

Table 9.3 shows parameters for four klystrons from SLAC — one S-band and three X-band, two using electromagnets and two with permanent magnets — and illustrates a number of the design differences within this class of tubes. First, the S-band klystron, with output power higher than the others by a factor of two or three, operates at the highest voltage and current, as

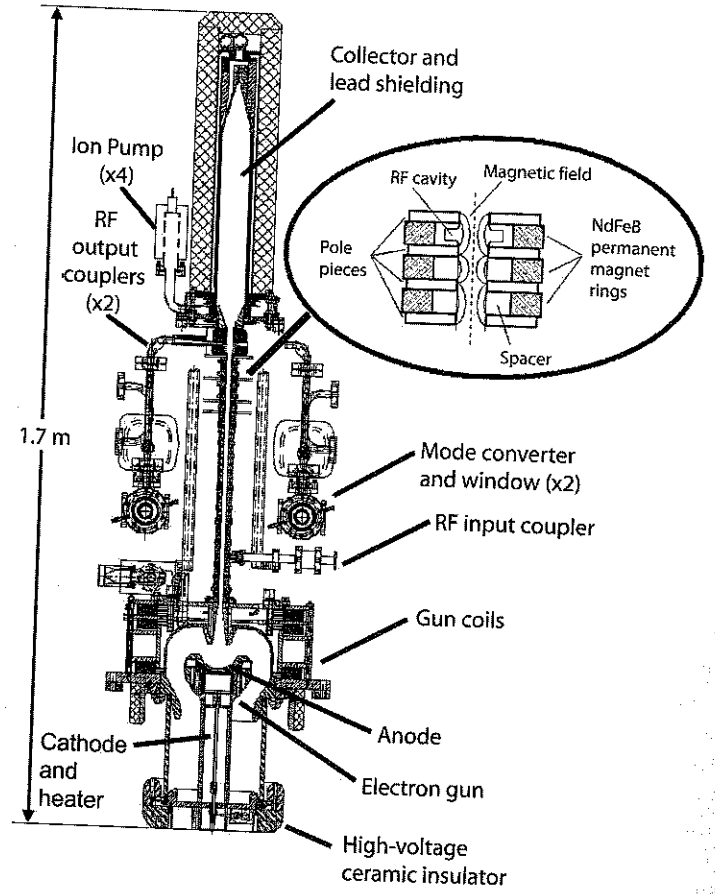

FIGURE 9.15
The 75-MW PP focused klystron (XP3 design).

TABLE 9.3

Comparison of the Second 150-MW S-Band Klystron Built by SLAC for DESY and Three X-Band Klystrons from SLAC, One with a Solenoidal Magnetic Field Coil and Two with PPM Focusing

	DESY, 150 MW	Solenoidal, 75 MW	PPM, 50 MW	PPM, 75 MW
Frequency, GHz	2.998	11.42	11.42	11.42
Beam voltage, kV	525	440	459	490
Beam current, A	704	350	205	274
Beam microperveance, $\mu A/V^{3/2}$	1.85	1.20	0.66	0.80
Cathode current density, A/cm^2	5.04	8.75	7.39	7.71
Cathode convergence	40:1	129:1	144:1	98:1
Axial magnetic field, T	0.20	0.45	0.20	0.17
Saturated gain	~55 dB	~55 dB	~55 dB	~55 dB
Efficiency	~50%	~50%	~60%	~55%

well as the highest perveance. While this makes more beam power available, there is a trade-off: the table shows that even though the gain for each klystron is about the same, the efficiency drops off with increasing perveance. Second, because the drift tube diameter scales approximately inversely with the frequency, the X-band tubes require considerably greater convergence in reducing the electron beam diameter from the cathode to the drift tube. This is the case despite the fact that the cathode current density is significantly higher for these tubes. Third, looking solely at the three X-band klystrons, the magnetic field in the PPM klystrons is half that for the tube with the electromagnet; i.e., the PPM klystrons operate closer to the Brillouin limit. This fact must be taken in context, though: the axial field for the electromagnet is roughly uniform with radius, while in the case of the permanent magnets, the radial dependence of the magnetic field within the drift tube is proportional to the modified Bessel function, $I_0(2\pi r/L)$, where L is the period of the magnetic field variation in the axial direction. This function increases with r from a value of unity on axis, behaving approximately like $\exp(2\pi r/L)/(4\pi^2 r/L)^{1/2}$ for large values of the argument. This behavior stiffens the beam, with a restoring force against radial displacements that increases with the size of the displacement.[34]

Finally, to put the energy savings using PPM technology into context, we consider the 75-MW X-band klystrons. Both are meant to operate at pulse lengths of $\tau_p = 1.5$ μsec and repetition rates of R = 180 Hz. Thus, the average microwave output is

$$\langle P_{\mu w} \rangle = P_{\mu w,peak} \tau_p R = 20.25 \text{ kW} \tag{9.31}$$

and the average beam power is

$$\langle P_{beam} \rangle = P_{beam,peak} \tau_p R = \frac{P_{\mu w,peak}}{\eta} \tau_p R \tag{9.32}$$

with η the beam-to-microwave power efficiency. The average beam power is 40.5 kW for the higher-perveance tube with an electromagnet and 36.8 kW for the PPM tube. However, the electromagnet adds an additional 25 kW,[31] so even ignoring the efficiency of converting prime power to electron beam power, the average power demand for the tube with an electromagnet is 65.5 kW, while that for the PPM tube is only 36.8 kW.

9.4.2 High-Impedance, Relativistic Klystrons

Truly relativistic klystrons with operating voltages well above 500 kV were considered as drivers for *two-beam accelerators* (TBAs),[35] in which microwaves generated in sources powered by a lower-voltage/higher-current beam were to be used to drive a higher-energy/lower-current beam in an RF linac to

very high energies. The central idea was to reuse the drive beam, passing it through a set of interaction cavities to generate microwaves, then reaccelerating it back to its original energy and cleaning it up to pass it through additional downstream interaction cavities to extract further microwave output. In the originally proposed concept, each drive beam was to be the source of energy for 150 klystrons, which were to be distributed over a distance of about 300 m, with each klystron producing 360 MW.

Two research teams explored the use of klystrons as the microwave source in a TBA, one from Lawrence Livermore National Laboratory (LLNL) and Lawrence Berkeley National Laboratory (LBNL) in the U.S. (with early participation from SLAC) and the other from the Budker Institute of Nuclear Physics (BINP) in Protvino and the Joint Institute of Nuclear Research (JINR) in Dubna, Russia. Both teams' programs were terminated before they were completed, but their work is the source of a great deal of useful research.

The U.S. team's work divides rather neatly into two phases. In the first, experimenters used standard velocity modulation techniques to initiate the bunching process in a single klystron, while in the second, they used a beam-chopping technique in which the beam was electromagnetically displaced back and forth across an aperture by time-varying fields to break the beam into bunches for injection into a series of extraction and reacceleration sections. Four basic device types were explored in the first phase of the work:[36-38]

- SL-3, a multicavity klystron using a conventional electron gun and operating at 8.6 GHz, three times the basic SLAC S-band klystron frequency
- SHARK (for subharmonic-drive klystron), a two-cavity klystron with a 5.7-GHz subharmonic drive and 11.4-GHz output
- SL-4, a high-gain relativistic klystron that produced the highest output power of about 300 MW
- SHARK-2, a three-cavity version of SHARK

As an example, consider the SL-4, shown in Figure 9.16. This configuration was used in the MOK-2 experiments (MOK standing for multi-output klystron), with output power tapped from both the penultimate and final cavities. The cavity parameters for MOK-2 are given in Table 9.4.[37] The penultimate cavity, designed both for power extraction and to further bunch the beam for the final cavity, is a standing wave cavity with a drift tube diameter of 11.4 mm; it is located 21 cm downstream of the final gain cavity. As shown in the table, its characteristic impedance, R/Q, is 175 Ω. To avoid breakdown in this cavity, its output was held below 100 MW. The final cavity is a traveling wave structure with a beam aperture diameter of 14 mm. It consists of six $2\pi/3$-mode cells, has an RF filling time* of about 1 nsec, and the group velocity through it tapers from about 94% of the speed of light at

* The filling time is the length of the structure divided by the group velocity of waves through the structure.

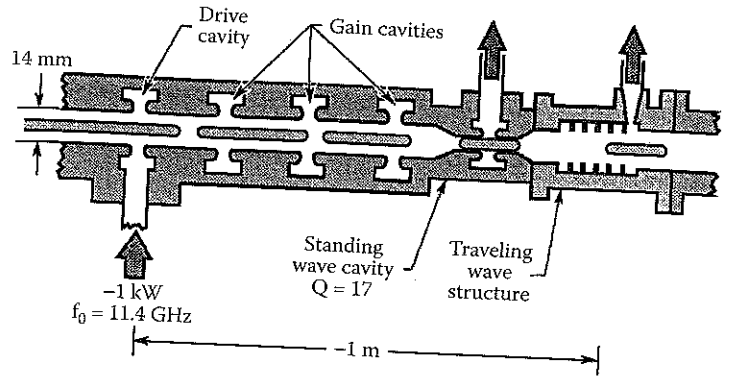

FIGURE 9.16
The SL-4 relativistic klystron used in the MOK-2 (Multi-Output Klystron) experiments. (From Allen, M.A. et al., *Part. Accel.*, 30, 189, 1990. With permission.)

TABLE 9.4

Cavity Parameters for MOK-2

Cavity Number	Cavity Type	Axial Location (cm)	$f - f_0$ (MHz)	Q^a	R/Q^b (Ω)
1	Drive	0	4	315	160
2	Gain	28	−31	117	160
3	Gain	42	23	122	160
4	Gain	63	45	119	160
5	Standing wave output	85	106	17	175
6	Traveling wave output	99[c]	0	—	—

Note: f_0 = 11.424 GHz.

[a] Beam-off Q.
[b] Calculated.
[c] To center of cell.

Source: From Allen, M.A. et al., Relativistic Klystrons, paper presented at the Particle Accelerator Conference, Chicago, 1989 (SLAC-PUB-4861; Lawrence Livermore National Laboratory, UCRL-100634; Lawrence Berkeley National Laboratory, LBL-27147; all 1989).

entry to about 90% at the output coupler, to raise efficiency by taking account of the loss of beam energy. At the designed output power level of 250 MW, voltage of 1.3 MV, and RF current of 520 A (*not* the DC current), the peak field level in the traveling wave coupler was to be limited to 40 MV/cm. In experiments, the maximum power extracted from the traveling wave structure itself was about 260 MW. The highest aggregate power from the two extraction cavities together was 290 MW, with 60 MW from the standing wave structure and 230 MW from the traveling wave structure. This latter was reached for a beam voltage and current of 1.3 MV and 600 A, respectively. Thus, for nominal input of 1 kW, the gain was about 55 dB and the efficiency was about 37%. Velocity spread in the injector, which became significant above 1.2 MV, was a limiting factor for the output power.

Comparison of Single Resonant Cavity and Traveling Wave Output Structures at 11.424 GHz

Parameter	Single Resonant Cavity		Traveling Wave Structure	
	Scaling	Value	Scaling	Value
Breakdown power	$1/g^2$	80 MW	$4/L^2$	460 MW[b]
Surface E-field[a]	$1/g$	190 MV/m	$2/L$	80 MV/m
Average E-field[a]	$\Delta V/g$	75 MV/m	$2\,\Delta V/L$	25 MV/m
Filling time	$4Q/\omega$	2 nsec to 95%	L/v_g	1 nsec to 100%
$(R/Q)_\perp$	g	20 Ω	L	100 Ω

Note: g is the gap width of the single resonant cavity, L is the length of the traveling wave structure, ΔV is the beam energy loss, v_g is the group velocity in the traveling wave structure, and $(R/Q)_\perp$ is the transverse mode impedance for the hybrid EM_{11} mode, which leads to breakup of the beam and its loss on the walls.

[a] Field at 80-MW power level.
[b] Extrapolated.

Source: Allen, M.A. et al., Relativistic Klystron Research for Linear Colliders, paper presented at the DPF Summer Study: Snowmass '88, High-Energy Physics in the 1990s, Snowmass, CO, 1988 (SLAC-PUB-4733, 1988).

The use of a traveling wave structure for the output, resulting in a twystron-like device, reduces the risk of breakdown, thereby reducing the peak electric fields by an amount proportional to the length of the structure. Table 9.5 compares output structure parameters and their scaling[36] with the gap width, g, for a single resonant cavity, or the traveling wave structure length, L. Note the favorable reductions of electric fields in the traveling wave structure, as well as the shortened filling time. Unfortunately, the scaling of the transverse mode impedance for the hybrid EH_{11} beam breakup mode is unfavorable, being a factor of five higher for the traveling wave structure. Therefore, additional measures must be taken in the construction of this device to avoid beam breakup problems and the attendant pulse shortening.

Although the second phase of experiments, which were to be performed on the relativistic klystron two-beam accelerator (RTA)[39] shown in Figure 9.17, were never actually conducted, the planned system illustrates the complexity of the relativistic klystrons required for this application. The RTA was laid out over a total distance of 24 m; a 1.2-kA, 1-MV electron beam was to be launched from a dispenser cathode and accelerated to 2.8 MeV before passing into a beam-chopping cavity, which was the same as that used earlier in a device called the Choppertron,[40] shown in Figure 9.18. In this chopper, a beam is deflected back and forth across an aperture by a rotating cavity mode, resulting in a chopped beam with a bunch frequency (11.4 GHz) twice that of the signal in the chopping cavity (5.7 GHz). The decision to use this modulation mechanism was driven by the reduced effect of velocity modulation on relativistic beams, as illustrated in Equation 9.11 or 9.15. To avoid excessive current loss in the chopping cavity, it was necessary that the current bunches

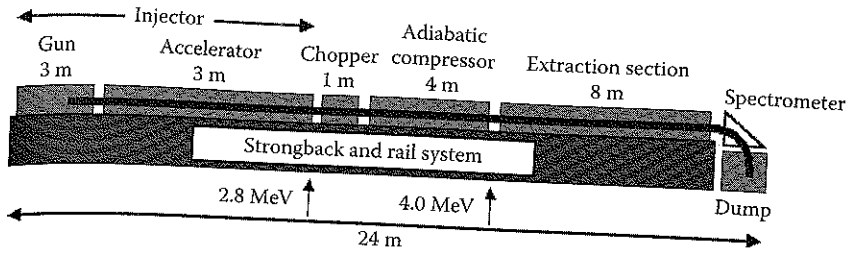

FIGURE 9.17
Layout of the relativistic klystron two-beam accelerator (RTA). (From Houck, T. et al., *IEEE Trans. Plasma Sci.*, 24, 938, 1996. With permission.)

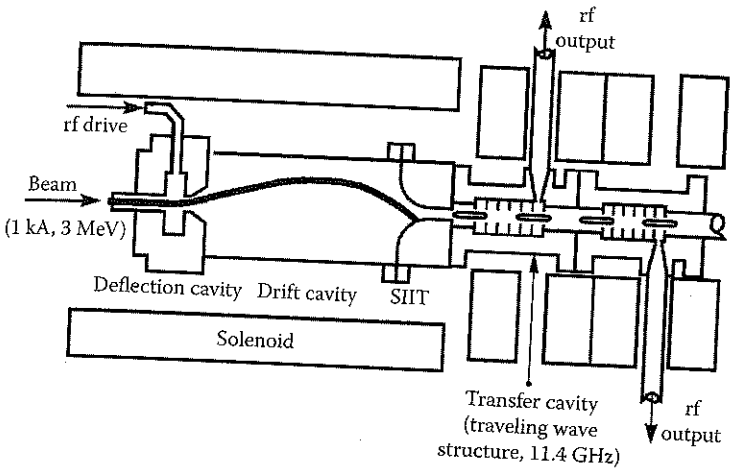

FIGURE 9.18
The Choppertron. The beam deflection cavity at the left was used later in the RTA. (From Allen, M.A. et al., *Part. Accel.*, 30, 189, 1990. With permission.)

created there be longer than desired in the final extraction section. Therefore, the next section of the RTA, the adiabatic compressor section, consisted of a set of additional accelerating cells interspersed with inductively tuned cavities, the latter included for the purpose of shortening the bunches (see Problem 21). The 4-MeV beam exiting the compressor section was to pass into an extraction section consisting of a set of eight klystron microwave extraction cells, each designed to produce 180 MW of 11.424-GHz output, interspersed with reacceleration cells to replace the beam energy lost in an extraction cell.

Ultimately, in a Two-Beam Next Linear Collider (TB-NLC) version (see Section 3.7), beam chopping and microwave extraction were to occur at 2.5 and 10 MeV, respectively. The klystron for that system was to produce 360 MW in the three-cell traveling wave output section shown in Figure 9.19. The beam into that section was to pass through a 16-mm-diameter drift tube with a DC current of 600 A and an RF current of 1150 A. Peak electric fields in the structure were to be 75 MV/m, and output coupling was through a pair of waveguides.

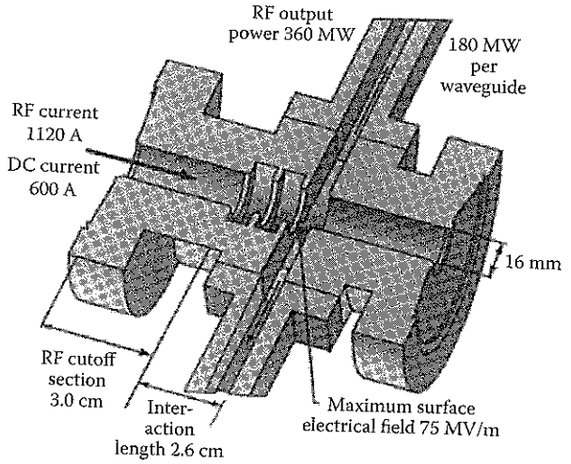

FIGURE 9.19
Planned output section for the proposed Two-Beam Next Linear Collider (TB-NLC). (From Houck, T. et al., *IEEE Trans. Plasma Sci.*, 24, 938, 1996. With permission.)

The key features of the work from BINP and JINR,[41] which has also been terminated, were the very large design gain, over 80 dB, and the large diameter of the drift tube for the beam. The large gain was necessitated by the system design goals of using a solid-state microwave source with an output power of order 1 W as the RF driver for the klystron, and obtaining an output power per klystron of about 100 MW. The design voltage was 1 MV, and the current was 250 A, for a microperveance of 0.25 (i.e., a perveance of 0.25×10^{-6} A/V$^{3/2}$), which is lower than that for the SLAC tubes of Table 9.3. To compare with the high-current annular-beam klystrons, this tube had 1 input cavity, 10 gain cavities, and a 22-cell traveling wave output structure; the total length was 70 cm.[42] Within the gain cavity region, PPM focusing of the beam was used, with a maximum field of 0.4 T and a root-mean-square (rms) average field of 0.28 T. The input cavity and each of the gain cavities were two-gap π-mode cavities with a loaded Q of 830. Output power was coupled out on both sides of the traveling wave output section. At a peak output power of 135 MW, the design value for the maximum surface electric field strength in the gain cavities was 300 kV/cm. The design gain was 83 dB and the efficiency 54%. The peak published power for the klystron was 100 MW.

With a relatively large drift tube diameter of 15 mm, the two lowest cutoff frequencies in the cylindrical drift tube between cavities, those for the TE_{11} and TM_{01} modes, are 11.7 and 15.3 GHz, respectively. The lower of these fell below the 14-GHz operating frequency for the klystron. Thus, the designers had to prevent parasitic oscillations in the TE_{11} mode of the beam tube so that it did not propagate through the system. The importance of suppressing this mode was heightened by the fact that its field pattern tends to drive the beam into the wall, terminating operation of the klystron. To accomplish this goal, a lossy waveguide section using a glass–carbon material was inserted between the gain cavities to suppress parasitic oscillations. In particular, between the 9th and 10th cavities, the designers inserted a special filter for the TE_{11} mode as an extra measure to suppress it. Measurements verified that the lossy waveguide sections quenched the TE_{11} parasitic oscillations.

9.4.3 Low-Impedance Klystrons

The intense annular-beam klystron, developed as the RKA at the Naval Research Laboratory,[43] underwent roughly three phases of development: (1) from the late 1980s to the early 1990s, when the original design concept was improved until a maximum power of about 15 GW at 1.3 GHz was achieved; (2) then up to the mid-1990s, with improvements in gap design and output coupling; and (3) from the mid-1990s to the present, with the initial and incomplete development of the triaxial configuration aimed at simultaneously achieving high currents at lower voltages while maintaining the cutoff condition for the beam drift tube (see Problem 25). In addition to the NRL work, this device has been explored by Physics International (now known as L3 Communications Pulse Sciences),[44] Los Alamos National Laboratory,[45] and the Air Force Research Laboratory, where a variant called the relativistic klystron oscillator (RKO) was developed.[46]

In the first stage of development, the RKA produced output powers in excess of 10 GW in the L-band, operating at 1.3 GHz, and in excess of 1 GW in the S-band, operating at 3.5 GHz.[47] Figure 9.20 shows a schematic diagram of the L-band device. The first cavity has a rather large radius to allow microwave signal injection around the foil-less diode into the first cavity; there is one additional bunching cavity, and the beam is collected on the end

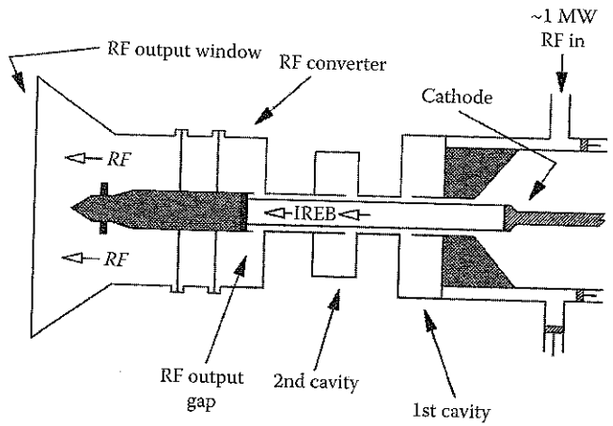

FIGURE 9.20
Schematic diagram of the NRL L-band RKA. (From Serlin, V. and Friedman, M., *IEEE Trans. Plasma Sci.*, 22, 692, 1994. With permission.)

TABLE 9.6

Comparison of Low-Impedance Klystrons from NRL Operating in the L- and S-Bands[47]

	L-Band (1.3 GHz)	S-Band (3.5 GHz)
Electron Beam		
Beam voltage (kV)	1000.0	~500
Beam current (kA)	35	~5
Beam pulse duration (nsec)	160	120
Beam mean radius (cm)	6.6	2.35
Beam thickness (mm)	4	N/A
Drift tube radius (cm)	7	2.4
First Cavity		
Computed gap voltage (kV)	50	~25
Cavity impedance (Ω)	~50	50
Cavity length (cm)	N/A	19
Distance to current maximum (cm)	39	12
RF current at peak (kA)	1.5	0.3
Second Cavity		
Cavity impedance (Ω)	10	20
Cavity length (cm)	17	11
Distance to current maximum (cm)	39	14
RF current at peak (kA)	17	5
Output power (GW)	15	1.7
Microwave pulse length (nsec)	N/A	40 (triangular pulse)
Power efficiency (%)	~40	~60

Note: N/A = not available.

of the suspended inner conductor of the coaxial output converter, in which a TEM-like mode coupled out through the extraction gap is converted to a TM_{01} output mode. Table 9.6 compares the key design and operating parameters for the L- and S-band devices producing the largest output powers. Note that the radii of the drift tubes vary in rough proportion to the operating frequency, which is to be expected on the basis of Equation 9.6. Similarly, because the cavities have the same impedances in each device [e.g., the driven cavity in each case has an impedance of about $Z_0 = 60 \ln(r_c/r_0)\ \Omega \approx 50\ \Omega$], the cavity radii scale with the frequency from one device to the other. On the other hand, the larger L-band device operates at higher voltage and current, as well as lower impedance. Further, the RF component of the current is much larger, and the output power is almost an order of magnitude higher than that of the S-band device.

Because of the rather large size of the cavities, they are able to support a number of modes, some lower in frequency than the operating frequency of the device. The designers addressed this issue in several ways. First, the driven and bunching cavities had different impedances and lengths to offset the competing modes. Thus, the two cavities were originally designed to have impedances of 50 Ω for the driven cavity and 20 Ω for the other (although, as we shall discuss, the impedance of the second cavity was later reduced in the L-band klystron). In the S-band klystron, the driven cavity had a length of about $(9/4)\lambda$, while the other had a length of about $(5/4)\lambda$ (see Equation 9.7); both, incidentally, were designed to be relatively narrow in the radial direction compared to their length in order to make their resonant modes more TEM-like. Mode control in the driven cavity of the L-band device was originally found to be dependent on the magnitude of the axial magnetic field, which was attributed to the fact that it was made of a nonmagnetic stainless steel with a weakly field-dependent permeability, μ. Lining the inner wall of the cavity with copper eliminated this problem. As an alternative means of mode control, thin, resistive nichrome wires were strung radially beween the inner and outer walls of the 20-Ω cavity in the S-band klystron at the axial location of the nodes in the field pattern for the mode resonant at the 3.5-GHz operating frequency, which reduced the Q for competing modes while leaving the Q of the resonant mode unaffected.

Beam bunching downstream of the first cavity, and the accompanying generation of an RF current component, proceeds as expected from the linear theory; in the L-band device

$$I_1(kA) = 1.5\sin(0.04z) \tag{9.33}$$

An oscilloscope trace of the measured current is shown in Figure 9.21. Earlier published data in a somewhat smaller, lower-power L-band klystron showed that the magnitude of the RF current was proportional to the square root of the input microwave power to the first cavity, which in turn is proportional to the magnitude of the gap voltage in the first cavity,[43] as expected.

As discussed in Section 9.3.5, when the gap voltage in the second cavity exceeds the threshold value given in Equation 9.18, a new mechanism creates

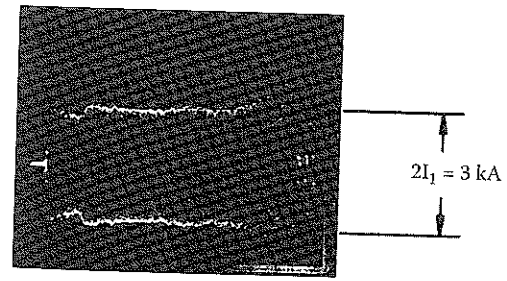

FIGURE 9.21
Oscilloscope trace of the envelope of the RF current I_1 at a distance beyond the first gap for which I_1 is a maximum. (From Serlin, V. and Friedman, M., *IEEE Trans. Plasma Sci.*, 22, 692, 1994. With permission.)

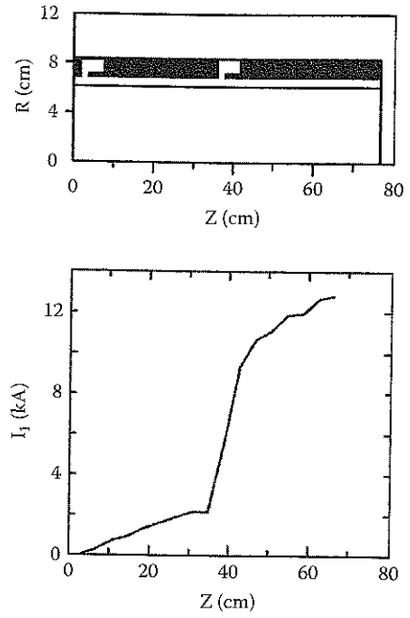

FIGURE 9.22
The geometry employed in computer simulations.of an L-band RKA, and the RF current as a function of distance along the simulation geometry. (From Friedman, M. et al., *Rev. Sci. Instrum.*, 61, 171, 1990. With permission.)

a time-periodic gate in the gap, which actually causes the slow space-charge wave on the beam to cease propagating, so that substantial additional bunching occurs in the immediate vicinity of the gap. Computer simulations shown in Figure 9.22 illustrate the process on a 16-kA beam accelerated in a 600-kV diode; the beam had a diameter of 12.6 cm and a thickness of 0.2 cm.[48] In the L-band experiments, the first gap at z = 2.8 cm was driven at 1.3 GHz, and at z = 30 cm, I_1 = 2.6 kA. Just 2 cm past the second gap, however, I_1 = 5.5 kA, and I_1 continues to increase with distance from the gap, reaching 12.8 kA at 34 cm beyond the gap.

In initial experiments with a 20-Ω second cavity, I_1 was lower than expectations, which was blamed on beam loading of the cavity. Lowering the second cavity impedance to 10 Ω, with provision for mechanical tuning of the cavity while in operation, pushed the RF current back up to a value of almost 17 kA, as shown in Figure 9.23 for a 6-GW, L-band RKA. Note that the rise of the current is still rather slow.

The output signal in Figure 9.24 rises more rapidly than I_1 in the previous figure, but it begins to drop off immediately after reaching its peak about 20 nsec into the 80-nsec pulse. Even at this lower power level, the electric fields near the tip of the converter in Figure 9.20 are approximately 500 kV/cm, and open-shutter photographs of the tip of the converter and the radiating

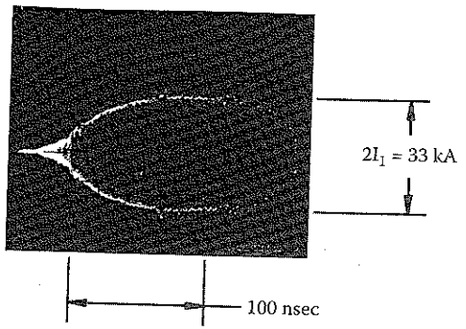

FIGURE 9.23
Oscilloscope trace of the envelope of the RF current I_1 at a distance beyond the second gap for which I_1 is a maximum. (From Serlin, V. and Friedman, M., *IEEE Trans. Plasma Sci.*, 22, 692, 1994. With permission.)

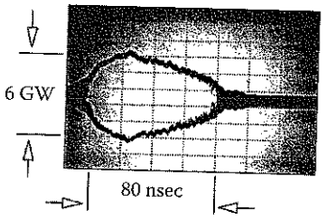

FIGURE 9.24
Oscilloscope trace of the RF signal extracted into the atmosphere. (From Serlin, V. and Friedman, M., *IEEE Trans. Plasma Sci.*, 22, 692, 1994. With permission.)

horn showed electron emission from the converter. At power levels near 15 GW, the fields near the converter tip were approximately 800 kV/cm, and the power levels were erratic.

The power output in the S-band device was initially disappointingly low: about 150 MW. The power was increased when a second, tunable cavity was added to share the output gap with the output converter carrying power to the antenna, as indicated in Figure 9.25. When the added cavity was tuned exactly to the output frequency, power was increased to the maximum of 1.7 GW. The stub shown at the left end of the center portion of the extraction section in Figure 9.20 provides a second tunable element in both extraction sections (we note that it was also used on the S-band klystron, although it is not shown in Figure 9.25). The reflection coefficient for radiation between the upstream and downstream sections of the extraction section is a function of the height and location of the tuning stub.[49]

The TM mode output of the design in Figure 9.20 has been converted into the useful rectangular TE_{01} mode using the method shown in Figure 9.26.[50] Radial fins are slowly introduced into the center conductor of the coax at the output end and grow until they reach the outer conductor, where they

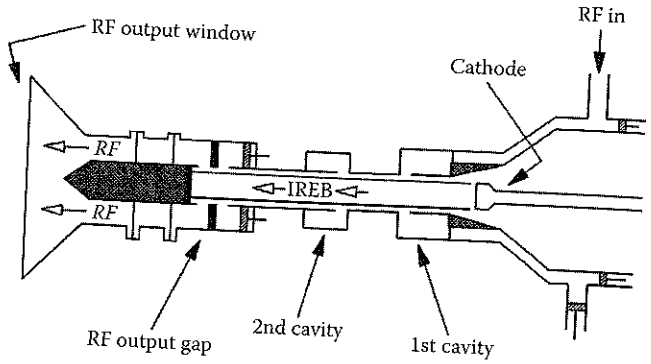

FIGURE 9.25
Schematic diagram of the NRL S-band RKA. (From Serlin, V. and Friedman, M., *IEEE Trans. Plasma Sci.*, 22, 692, 1994. With permission.)

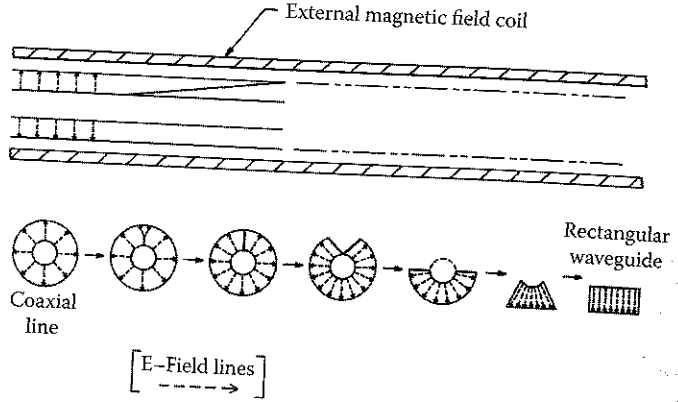

FIGURE 9.26
Mode converter smoothly changes a TM mode to a rectangular TE_{01} mode at the output of the relativistic klystron. (From Serlin, V. et al., *Proc. SPIE*, 1407, 8, 1991. With permission.)

divide and adiabatically transform into a rectangular cross section. Such a converter has been built for a high-current S-band klystron[51] and has been operated at 20 MW, although it suffered from breakdown due to short transition sections.

At the end of this first phase of development, the NRL team identified five problem areas to be addressed in the further development of their low-impedance klystrons:[51] (1) alignment of the drift region, the electron beam, and the axial magnetic field; (2) magnetic field uniformity; (3) beam loading of the cavities; (4) vacuum quality; and (5) x-ray bombardment. In the case of magnetic field uniformity, for example, they derived a requirement on the maximum allowable variation in the axial magnetic field,

$$\Delta B_z = 2B_z\left(\frac{r_0 - r_b}{r_b}\right) \tag{9.34}$$

They noted that while this uniformity is easily achieved with a DC magnetic field, the use of pulsed electromagnetic field coils requires that one take account of eddy currents, skin depth, and magnetic field penetration through materials, which typically translates to a requirement on the pulse length for the magnet. In the case of the vacuum quality, they commented that the vacuum level of 10^{-5} torr, customary for pulsed power experiments, was inadequate at the highest power, with the result that breakdown could be observed in either or both of the cavities, as well as in the converter region, and that electron beam propagation could become unstable. The x-ray dose generated in a relativistic electron beam system, which scales roughly as $V_0^3 I_b$, with V_0 the accelerating voltage, necessitates the use of heavy shielding and creates additional breakdown problems in the klystron due to x-rays hitting the wall, producing electrons. To reduce the dose, one can reduce the operating voltage and increase the current proportionately, so that the dose decreases as V_0^{-2}. To achieve that goal, the triaxial klystron was pursued in the third stage of development, which we will describe in Section 9.5. Here, though, we describe the second phase of development, which addressed beam loading of the cavities as well as the conversion of electrostatic potential energy to beam kinetic energy in order to increase efficiency.

Two major steps were taken during the second phase of RKA development. First, the gaps in the klystron cavities were opened up considerably, and a cavity field pattern featuring a reversal of the axial electric field in the gap was employed, as indicated in Figure 9.27.[52] To prevent the buildup of electrostatic potential energy in the effectively wider drift tube in the vicinity of the gap, metallic washers connected by thin conducting rods acting like inductors were placed in the gap. Therefore, the gap was shorted out for the DC component of the beam current, while it was open to the RF component of the current. The wider gap reduced gap capacitance and beam loading; it also reduced cavity Q, thus increasing the bandwidth of the device. The washer structure prevented the penetration of radial electric field components, but allowed the penetration of the azimuthal magnetic field, which had the fortuitous effect of allowing the generation of an inductive electric field component that heightened the bunching effects in the second RKA cavity. In experiments comparing wide- and narrow-gap RKAs, the former produced much higher RF current components for the same beam; results are shown in Table 9.7.

The second step was the tapered reduction of the inner radii of the washers in the extraction gap to recover a portion of the potential energy stored in the decreasing gap between the beam and the wall, converting it into kinetic energy of the beam electrons, which could in turn be converted to microwave energy and extracted.[53] Remarkably, a device with this feature operated more efficiently at a low axial magnetic field, with 60% power efficiency and 50%

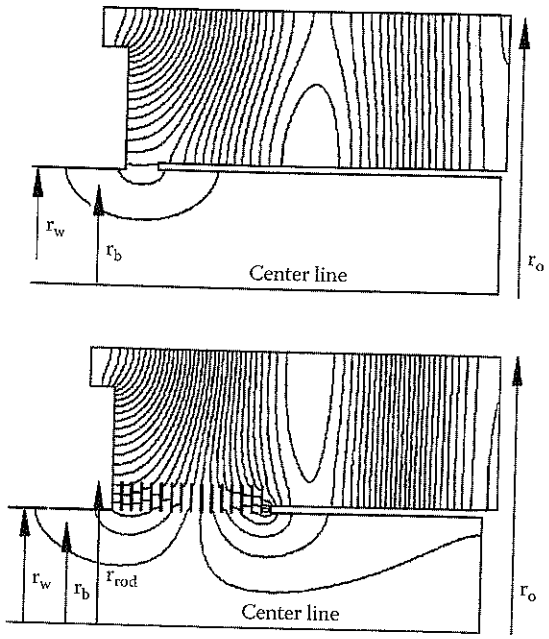

FIGURE 9.27
Electric field line calculations with SUPERFISH for narrow (upper) and wide (lower) gaps. (From Friedman, M. et al., *Phys. Rev. Lett.*, 74, 322, 1995. With permission.)

energy efficiency at 0.3 T; at 0.8 T, the output pulse length was considerably shorter, resulting in a lower energy efficiency. The reason was that at the lower magnetic field, electrons slowed by giving energy up to the microwaves were lost to the washers, while at the stronger magnetic field, those electrons remained in the gap, continuing to absorb microwave energy.

9.4.4 Reltrons

Reltrons are a compact source offering high efficiencies of 30 to 40% and a wide range of operating frequencies, from UHF (700 MHz) to X-band (12 GHz). This broad range was achieved in a system using several interchangeable modulating cavities and output sections at the fundamental frequency and multiples of two and three times the fundamental frequency.[54] An L-band reltron is shown in Figure 9.28. In L-band experiments, a 250-kV, 1.35-kA electron beam was bunched and then postaccelerated an additional 850 kV to produce a 600-MW microwave output at 1 GHz. The efficiency of converting electron beam power to microwave power output was about 40%. Pulse energy in the microwaves was about 200 J. Data from a long-pulse experiment in the L-band with output power of 100 MW over a pulse length of about 1 μsec are shown in Figure 9.29 (see Problem 26). Note that the microwave power begins about 200 nsec after the electron beam is injected. This time delay is the filling time of the modulation cavity, $\tau_f = Q/\omega$.

TABLE 9.7

Comparison of Wide- and Narrow-Gap RKAs

	Wide Gaps	Narrow Gaps
Beam current (kA)	16	16
Diode voltage (kV)	500	500
Beam mean radius (cm)	6.3	6.3
Drift tube radius (cm)	6.7	6.7
Washer inner radius (cm)	6.7	—
Washer outer radius (cm)	9.2	—
Washer thickness (cm)	0.075	—
Number of washers	23	—
First Cavity		
Gap width (cm)	10	~2
Q	~200	1000
RF current (kA)	4	5
Bandwidth	±5 MHz reduces RF current by 20%	<1 MHz reduces RF by 50%
Second Cavity		
Gap width (cm)	10	~2
Q	~450	1000
RF current (kA)	>40	14
Bandwidth	~3 MHz	—

Source: From Friedman, M. et al., Intense electron beam modulation by inductively loaded wide gaps for relativistic klystron amplifiers, *Phys. Rev. Lett.*, 74, 322, 1995.

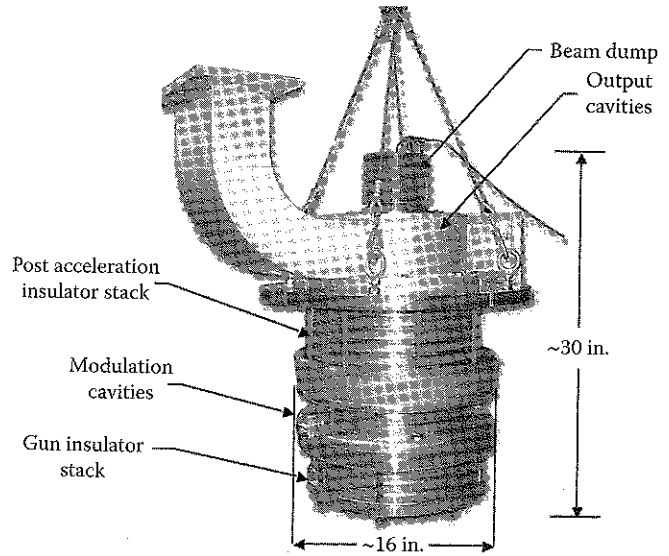

FIGURE 9.28
An L-band reltron. (Photograph provided by L3 Communications Pulse Sciences.)